Monthly Notices of the ROYAL ASTRONOMICAL SOCIETY

MNRAS **465,** 3134–3142 (2017) doi:10.1093/mnras/stw2912
Advance Access publication 2016 November 10

Dark-ages reionization and galaxy-formation simulation – VII. The sizes of high-redshift galaxies

Chuanwu Liu,[1]★ Simon J. Mutch,[1]★ Gregory B. Poole,[1] P. W. Angel,[1] Alan R. Duffy,[2] Paul M. Geil,[1] Andrei Mesinger[3] and J. Stuart B. Wyithe[1]★

[1]*School of Physics, University of Melbourne, Parkville, VIC 3010, Australia*
[2]*Centre for Astrophysics and Supercomputing, Swinburne University of Technology, PO Box 218, Hawthorn, VIC 3122, Australia*
[3]*Scuola Normale Superiore, Piazza dei Cavalieri 7, I-56126 Pisa, Italy*

Accepted 2016 November 8. Received 2016 November 6; in original form 2016 August 2

ABSTRACT

We investigate high-redshift galaxy sizes using a semi-analytic model constructed for the Dark-ages Reionization And Galaxy-formation Observables from Numerical Simulation project. Our fiducial model, including strong feedback from supernovae and photoionization background, accurately reproduces the evolution of the stellar mass function and ultraviolet (UV) luminosity function. Using this model, we study the size–luminosity relation of galaxies and find that the effective radius scales with UV luminosity as $R_e \propto L^{0.25}$ at $z \sim 5$–9. We show that recently discovered very luminous galaxies at $z \sim 7$ and 11 lie on our predicted size–luminosity relations. We find that a significant fraction of galaxies at $z > 8$ will not be resolved by *James Webb Space Telescope*, but Giant Magellan Telescope will have the ability to resolve all galaxies in haloes above the atomic cooling limit. We show that our fiducial model successfully reproduces the redshift evolution of average galaxy sizes at $z > 5$. We also explore galaxy sizes in models without supernova feedback. The no-supernova feedback models produce galaxy sizes that are smaller than observations. We therefore confirm that supernova feedback plays an important role in determining the size–luminosity relation of galaxies and its redshift evolution during reionization.

Key words: galaxies: evolution – galaxies: formation – galaxies: fundamental parameters – galaxies: high-redshift – galaxies: structure.

1 INTRODUCTION

The evolution of galaxy size during the Epoch of Reionization (EoR) provides an additional probe for understanding galaxy formation in the early Universe. In the hierarchical structure formation scenario (White & Rees 1978), dark matter haloes form first, then baryonic gas cools and falls into their potential wells to form galaxies. Within this scheme, Fall & Efstathiou (1980) studied the formation of galaxy discs. In this model, the spin of a rotationally supported galaxy disc originates from the conservation of angular momentum during the collapse of cooling gas. Further analytic modelling by Mo, Mao & White (1998) provided a relation between the disc scalelength of a galaxy, R_d, and the virial radius of its dark matter halo, R_{vir} for infinitesimally thin discs with exponential surface density profiles. The disc size can be written as

$$R_d = \frac{\lambda}{\sqrt{2}} \left(\frac{j_d}{m_d} \right) R_{vir}, \quad (1)$$

where m_d and j_d are the fractions of mass and angular momentum in the disc relative to the halo and λ is the spin parameter of the halo, which is a dimensionless measure of the angular momentum of the system.

The virial radius of a dark matter halo scales with redshift and virial velocity, V_{vir}, or virial mass, M_{vir}, as

$$R_{vir} = \left(\frac{GM_{vir}}{100H^2(z)} \right)^{1/3} = \frac{V_{vir}}{10H(z)}, \quad (2)$$

where $H(z)$ is the Hubble parameter, and $H(z) \propto (1+z)^{3/2}$ at high redshifts (Carroll, Press & Turner 1992). Therefore, from equation (1), the proportionality of R_d with R_{vir} predicts that the sizes of discs scale with redshift as $(1+z)^{-3/2}$ at fixed circular velocity or $(1+z)^{-1}$ at fixed halo mass.

Observations of Lyman break galaxies (LBGs) show that galaxies are more compact at higher redshift, and that average sizes evolve with redshift as $(1+z)^{-m}$ with $m \sim 1$–1.5 (e.g. Bouwens et al. 2004; Ferguson et al. 2004; Oesch et al. 2010; Grazian et al. 2012; Ono et al. 2013; Holwerda et al. 2015; Kawamata et al. 2015; Shibuya, Ouchi & Harikane 2015). Some recent observations of the redshift evolution of galaxy sizes are summarized in Table 1.

★ E-mail: chuanwul@student.unimelb.edu.au (CL); smutch@unimelb.edu.au (SJM); swyithe@unimelb.edu.au (JSBW)

Table 1. Observed evolution of galaxy sizes, $R_e \propto (1+z)^m$ from literature, where $L^*_{z=3}$ corresponds to UV magnitude $M_{UV} = -21.0$.

z	m	Sources
$L = (0.3-1)L^*_{z=3}$		
2–6	1.05 ± 0.21	Bouwens et al. (2004)
2–8	1.12 ± 0.17	Oesch et al. (2010)
2–12	1.30 ± 0.13	Ono et al. (2013)
2.5–12	1.24 ± 0.10	Kawamata et al. (2015)
0.5–10	1.10 ± 0.06	Shibuya et al. (2015)
5–10	1.32 ± 0.43	Holwerda et al. (2015)
$L = (0.12-0.3)L^*_{z=3}$		
2–8	1.32 ± 0.52	Oesch et al. (2010)
2–12	1.30 ± 0.13	Ono et al. (2013)
0.5–10	1.22 ± 0.05	Shibuya et al. (2015)
5–10	0.76 ± 0.12	Holwerda et al. (2015)

Semi-analytic models have had considerable success studying the formation and evolution of galaxies in the past two decades (e.g. White & Frenk 1991; Kauffmann, White & Guiderdoni 1993; Cole et al. 2000; Bower et al. 2006; Croton et al. 2006; Lacey et al. 2011, 2016). Galaxy sizes are important for semi-analytic models since the cold gas is assumed to settle in discs where star formation occurs at a rate depending on the surface density (e.g. Croton et al. 2006). Reproducing the evolution of galaxy sizes in the early and dense Universe is therefore important for semi-analytic models of reionization. On the other hand, feedback mechanisms are already known to play an important role in suppressing star formation in galaxies.

Using the observed size evolution and the luminosity function of galaxies, Wyithe & Loeb (2011) presented a simple model to constrain the feedback mechanism using galaxy sizes:

$$R_e \propto L^{\frac{1}{3(1+a)}}(1+z)^{-m}. \quad (3)$$

Here L is the galaxy luminosity, and a and m are free parameters which can be constrained using both the slope of the galaxy-luminosity function and galaxy-size evolution. Feedback arising from energy release and momentum outflow could affect the luminosity at fixed disc sizes. Based on the observed relation between size, luminosity and redshift, Wyithe & Loeb (2011) ruled out the no-supernova feedback model with high confidence, and suggested a supernova feedback model through the transfer of momentum. Here we improve on this analysis using a more realistic semi-analytic model. Investigation of galaxy sizes using semi-analytic models have previously been made using galaxies in both the local and high-redshift Universe (e.g. Cole et al. 2000; González et al. 2009; Shankar et al. 2010; Xie et al. 2015; Stevens, Croton & Mutch 2016; Tonini et al. 2016). Our purpose-designed semi-analytic model provides a tool to study galaxy sizes during the EoR.

The semi-analytic model, MERAXES (described in Mutch et al. 2016a, hereafter Paper-III), is a new purpose-built galaxy-formation model designed for studying galaxy evolution during the EoR.[1] MERAXES includes a temporally and spatially coupled treatment of reionization, and is built upon the high-resolution and high snapshot-cadence *N*-body simulation *Tiamat* (Poole et al. 2016, hereafter Paper-I). MERAXES successfully reproduces a series of high-redshift galaxy observables including the stellar mass function (Paper-III) and ultraviolet (UV) luminosity function (Liu et al. 2016, hereafter Paper-IV). In this paper, we run simulations to investigate the size–luminosity relation, the size–stellar mass relation and the redshift evolution of galaxy sizes at $5 < z < 10$. We aim to use the evolution of galaxy sizes to probe the physics of galaxy formation during the EoR. In particular, we study how sensitive galaxy sizes are to feedback, especially from supernovae feedback during the EoR.

This paper is organized as follows. In Section 2, we briefly introduce the semi-analytic model and *N*-body simulation used in this work. In Section 3, we study the relation between sizes and UV luminosities of galaxies. In Section 4, we discuss the probability of resolving galaxies using *Hubble Space Telescope (HST)*, *James Webb Space Telescope (JWST)* and Giant Magellan Telescope (GMT). In Section 5, we study the size–stellar mass relation of model galaxies. In Section 6, we present the redshift evolution of galaxy sizes and compare this with observations. In Section 7, we discuss the interpretation of our model sizes in the context of recent high-redshift observations. In Section 8, we present our conclusions. Throughout this work, we employ a standard spatially flat Λ cold dark matter cosmology based on *Planck* 2015 data (Planck Collaboration 2015): $(h, \Omega_m, \Omega_b, \Omega_\Lambda, \sigma_8, n_s) = (0.678, 0.308, 0.0484, 0.692, 0.815, 0.968)$. All magnitudes in this paper are presented in the AB system (Oke & Gunn 1983). The unit of luminosity, $L^*_{z=3}$, is the characteristic luminosity at $z \sim 3$, which corresponds to $M_{1600} = -21.0$ (Steidel et al. 1999).

2 SIMULATION AND MODELLING

The galaxy-formation model used in this work is MERAXES (Paper-III). MERAXES is implemented upon dark matter halo merger trees generated from the cosmological *N*-body simulation *Tiamat* (Paper-I). *Tiamat* and MERAXES have special features designed for the study of reionization.

2.1 *N*-body simulation

The collisionless *N*-body simulation, *Tiamat*, was run using a modified version of GADGET-2 (Springel 2005) and the *Planck* 2015 cosmology (Planck Collaboration 2015). It includes 2160^3 particles in a comoving 100 Mpc cube box. The mass of each particle is $2.64 \times 10^6\, h^{-1}\, M_\odot$, which allows us to identify the low-mass dark matter haloes close to the hydrogen cooling limit across the redshifts relevant to reionization. Dark matter halo finding was carried out using SUBFIND code (Springel et al. 2001). This code first identifies dark matter collapsed regions by a friends-of-friends (FoF) algorithm using a link length criterion of 0.2 times of the mean interparticle separation. The self-bound substructures are subsequently identified within these FoF groups as locally overdense collections of dark matter particles, removing unbound particles through an unbinding procedure. An FoF group typically contains a central halo holding most of the virial mass and a group of lower mass subhaloes which trace the undigested parts of merger events.

Tiamat outputs include 100 snapshots from $z = 35$ to 5 with a temporal resolution of 11 Myr per snapshot. This high cadence resolves the dynamical time of galaxy discs at high redshift, and is comparable to the lifetime of massive stars. Dark matter halo merger trees constructed from *Tiamat* are stored and processed in a 'horizontal' form. This allows the semi-analytic model to implement

[1] The MERAXES model is a part of the Dark-ages Reionization And Galaxy-formation Observables from Numerical Simulation (DRAGONS) project, http://dragons.ph.unimelb.edu.au.

a self-consistent calculation of feedback from reionization on low-mass galaxy formation. This is achieved by incorporating the semi-numerical reionization algorithm 21CMFAST (Mesinger, Furlanetto & Cen 2011) at each snapshot.

2.2 Semi-analytic model

MERAXES is a new semi-analytic model based on Croton et al. (2006) with updated physics for application to $z > 6$. It consists of baryonic infall, gas cooling, star formation, stellar mass recycling, metal enrichment, galaxy mergers, gas stripping and feedback from both supernova and reionization. To model the formation and evolution of galaxies during the EoR, MERAXES incorporates several improvements in the feedback scheme. First, it considers a delayed supernova feedback mechanism. In an instantaneous feedback scheme, a massive star instantly produces a supernova and so releases energy and mass within the same snapshot that the progenitor star formed. This is appropriate at low redshift, where the stellar lifetime is short compared to the galaxy dynamical time. However, our *Tiamat* merger trees have a much higher time resolution of ∼11 Myr, which is shorter than the lifetime of the least massive Type II supernova progenitor stars (e.g. ∼40 Myr for 8 $M_\odot$ stars). Therefore, MERAXES implements a delayed supernova feedback scheme, where a supernova may explode several snapshots after the progenitor star formed. MERAXES also includes feedback from a spatially and temporarily variable ultraviolet background (UVB). The UVB radiation heats the intergalactic medium and reduces baryonic infall within small dark matter haloes suppressing both gas cooling and star formation. To achieve this, MERAXES integrates the seminumerical code 21CMFAST (Mesinger et al. 2011) to construct the reionization structure.

We assume a standard Salpeter (1955) initial mass function with stellar mass in the range of $0.1 < m_* < 120\,M_\odot$:

$$\phi(m_*) \propto m_*^{-2.35}. \tag{4}$$

The free parameters in MERAXES were calibrated to replicate the observed stellar mass functions at $z \sim 5$–7 (González et al. 2011; Duncan et al. 2014; Grazian et al. 2015; Song et al. 2016) and the *Planck* optical depth to electron scattering measurements (Planck Collaboration 2015). For a more detailed description of MERAXES, see Paper-III.

2.3 Disc sizes and star formation

In our semi-analytic model, we adopt the disc scale radius from Mo et al. (1998) as shown in equation (1), and the standard assumption $j_d/m_d = 1$ (Fall & Efstathiou 1980), for which the specific angular momentum of the material forming the disc is the same as that of the host halo.

The spin parameter, λ, is calculated from the *N*-body simulation using the definition (Bullock et al. 2001):

$$\lambda = \frac{J_{\rm vir}}{\sqrt{2} M_{\rm vir} V_{\rm vir} R_{\rm vir}}, \tag{5}$$

where $M_{\rm vir}$ and $J_{\rm vir}$ are the mass and angular momentum enclosed within the virial radius,[2] $R_{\rm vir}$, and $V_{\rm vir} = \sqrt{G M_{\rm vir}/R_{\rm vir}}$ is the circular velocity at $R_{\rm vir}$ (see Angel et al. 2016, for a discussion of spin parameters for haloes in *Tiamat*).

Equation (1) was obtained assuming a simple model in which dark matter haloes have singular spherical isothermal density profiles and the gravitational effects of baryonic discs are neglected. It is therefore important to note that inclusion of gravity from the disc may alter the size and rotation curve of galaxies and modify the dark matter concentration in the inner region of the halo. However, Mo et al. (1998) showed that a more realistic model with NFW halo profiles (Navarro, Frenk & White 1997) and self-gravitating discs results in only minor modifications to equation (1).

Simulations also show that inclusion of the self-gravity of discs will lead to instabilities of gas and stars, which drives disc material towards the centre of galaxies and results in instability-driven star bursts and bulge growth in galaxies. This will have an impact on the distribution of disc sizes (e.g. Cole et al. 2000; Bower et al. 2006; Stevens et al. 2016; Tonini et al. 2016). Another significant assumption in the model is $j_d/m_d = 1$, since lots of angular momentum in the gas component lost during galaxy assembly would lead to a smaller disc. On the other hand, strong feedback mechanisms which release the energy and angular momentum to the interstellar medium will suppress the formation of small discs.

To quantify these effects in semi-analytic models, Guo et al. (2016) compared galaxy sizes from semi-analytic models L-GALAXIES and GALFORM at $z < 2$. GALFORM includes the self-gravity of discs while L-GALAXIES ignores it. Guo et al. (2016) showed that self-gravity does not significantly affect the sizes of galaxies with $M_* < 10^{9.5}\,M_\odot$. However, for galaxies with $M_* > 10^{9.5}\,M_\odot$, self-gravity of discs in GALFORM reduces galaxy sizes and results in a decreasing size–mass relation. In this work, which considers the small galaxies that drive reionization, we do not have a large number of galaxies with $M_* > M^{9.5}\,M_\odot$ at $z > 6$. Thus, we utilize the simple model of Mo et al. (1998) in this study, as has been common in semi-analytic models (e.g. Croton et al. 2006; De Lucia & Blaizot 2007).

From equations (1) and (5), we see that the disc sizes of galaxies are determined by the properties of dark matter haloes. We assume that star formation and feedback processes do not directly modify the disc sizes. On the other hand, the size of the disc does play a fundamental role in the buildup of stellar mass. In our model, freshly accreted baryonic matter in dark matter haloes is initially in the form of hot gas, and is assumed to follow a singular isothermal sphere density profile. The cold gas, which cools from the hot gas reservoir of the host FoF group, is assumed to fall on to the galaxy hosted by the central halo. MERAXES assumes that the cold gas settles in a rotationally supported disc with an exponential surface density profile. Based on the observational work of Kennicutt (1998), the global star formation rate of spiral galaxies can be related to the surface density of cold gas above a given threshold. In our model, we adopt a critical surface density for the disc, above which gas cannot maintain stability and will start forming stars. The critical density at a radius r is adopted from Kauffmann (1996),

$$\Sigma_{\rm crit}(r) = \Sigma_{\rm norm} \left(\frac{V_{\rm vir}}{\rm km\,s^{-1}}\right) \left(\frac{r}{\rm kpc}\right)^{-1} M_\odot\,{\rm pc}^{-2}, \tag{6}$$

where $\Sigma_{\rm norm} = 0.2$ is a free parameter in MERAXES. Stars are assumed to form within a maximum radius set to $R_{\rm disc} = 3R_d$ based on the properties of the Milky Way (van den Bergh 2000). By integrating $\Sigma_{\rm crit}$ to $R_{\rm disc} = R_d$, we obtain the critical mass of the disc,

$$m_{\rm crit} = 2\pi\Sigma_{\rm norm} \left(\frac{V_{\rm vir}}{\rm km\,s^{-1}}\right) \left(\frac{R_{\rm disc}}{\rm kpc}\right) 10^6\,M_\odot. \tag{7}$$

[2] $R_{\rm vir}$ is defined as that within which the mean density is $\Delta = 18\pi^2 + 82(\Omega_m(z) - 1) - 39(\Omega_m(z) - 1)^2$ times the critical density, ρ_c (Bryan & Norman 1998).

If the mass of cold gas in the disc, $m_{\rm cold}$, exceeds this threshold mass, the stars will form with a star formation rate given by

$$\dot{m}_* = \alpha_{\rm SF} \frac{m_{\rm cold} - m_{\rm crit}}{t_{\rm dyn}^{\rm disc}}, \quad (8)$$

where $\alpha_{\rm SF} = 0.03$ is a free parameter describing the star formation efficiency and $t_{\rm dyn}^{\rm disc} = R_{\rm d}/V_{\rm vir}$ is the dynamical time of the disc.

Galaxy mergers can also trigger a strong burst of star formation. We assume a fraction of the total cold gas of the newly formed system is consumed during such a burst (Somerville, Primack & Faber 2001)

$$e_{\rm burst} = \alpha_{\rm burst} \left(\frac{m_{\rm small}}{m_{\rm big}} \right)^{\gamma_{\rm burst}}, \quad (9)$$

where $m_{\rm small}/m_{\rm big}$ is the mass ratio of merging galaxies, and $\alpha_{\rm burst} = 0.56$ and $\gamma_{\rm burst} = 0.7$ are chosen to fit the numerical results of Cox et al. (2004) and Mihos & Hernquist (1994, 1996) for merger mass ratio in the range 0.1–1.0 (Croton et al. 2006). For simplicity, we assume the merger-driven burst occurs within a single snapshot, which is comparable to the disc dynamical time of the majority of galaxies. We do not consider irregular morphologies during galaxy mergers and the sizes of remnants are calculated using equation (1).

Through the star formation process, disc size affects a number of galaxy properties, including UV luminosities. The size–luminosity relation therefore becomes an important predictor from galaxy-formation models. We note that the star-forming process is rather complicated. It is not only determined by the galaxy sizes but also by other effects including cooling, mergers and feedback. To study the role of supernova feedback in the buildup of the size–luminosity (stellar mass) relation, we also run a simulation with the supernova feedback switched off. This no-supernova model cannot reproduce the stellar mass function in detail, but is recalibrated to provide the observed stellar mass density at $z = 5$ (see Paper-III).

In this paper, to compare with observations, we present the sizes of model galaxies using the physical effective radius (i.e. half-light radius), $R_{\rm e}$, within which half of the galaxy's luminosity originates. Here $R_{\rm e}$ is estimated using $R_{\rm e} = 1.678 R_{\rm d}$, where the constant originates from the assumed exponential surface density profile and constant mass-to-light ratio.

2.4 UV luminosities

Luminosity is the most direct observable of high-redshift galaxies. We calculate the UV luminosities using stellar population synthesis. For each galaxy, we obtain the stellar population components by tracking its star formation and merger history. We integrate the stellar populations with model spectral energy distributions calculated using STARBURST99 (Leitherer et al. 1999; Vázquez & Leitherer 2005; Leitherer et al. 2010, 2014) with a constant metallicity of $Z = 0.05\,{\rm Z}_\odot$. We do not include nebular components as they would not affect the UV luminosities of our model galaxies at these redshifts.

To obtain the observed luminosities, we apply a dust extinction model to each galaxy. We adopt a luminosity-dependent dust model (e.g. Smit et al. 2012; Bouwens et al. 2015), which is based on the IRX-β relation from Meurer, Heckman & Calzetti (1999) and the observed luminosity-β relation from Bouwens et al. (2014). This dust model is empirical and is calibrated to reproduce the observed properties of galaxies. For more details about the galaxy photometric modelling see Paper-IV.

3 SIZE–LUMINOSITY RELATION

We first investigate the relationship between the physical size and UV luminosity of model galaxies. Fig. 1 shows the relation between the effective radius and UV magnitude $M_{\rm UV}$ for model galaxies at $z \sim 5$–10, where the UV magnitude $M_{\rm UV}$ is the dust-extincted luminosity at the rest frame 1600 Å. We see that at $M_{\rm UV} \lesssim -14$, galaxies with brighter UV luminosity tend to have larger sizes.

We note that the effective radius does not significantly change with luminosity for the galaxies with luminosities $M_{\rm UV} > -14$. This is because galaxies fainter than $M_{\rm UV} \sim -14$ are located in the dark matter haloes of the minimum gas cooling mass. This is similar to the turnover at $M_{\rm UV} \sim -14$ in the relation between UV luminosity and the mass of dark haloes found in Paper-IV. We see that at fixed luminosity, the size of galaxies grows from $z \sim 10$ to 5. We discuss the redshift evolution of galaxy sizes further in Section 6.

For comparison with our simulations, we show the observed $R_{\rm e}$–$M_{\rm UV}$ relations from Huang et al. (2013) at $z \sim 5$ and Shibuya et al. (2015) at $z \sim 5$–8, where the latter is calculated by us using the sizes data from Shibuya et al. (2015). Our results are in close agreement with the observations.

Recently, Oesch et al. (2016) found an unexpectedly luminous galaxy (GN-z11) at $z \sim 11$, which has $M_{\rm UV} = -22.1 \pm 0.2$ and $R_{\rm e} = 0.6 \pm 0.3$ kpc. In Mutch et al. (2016b), we demonstrated that the properties of GN-z11 are in good agreement with the results of our model in terms of stellar mass, star formation rate and UV luminosities. We show the measured size of GN-z11 in Fig. 1 and we find that it is in agreement with our fitted size–luminosity relation at $z \sim 10$.

The relation between the galaxy size and luminosity is commonly fitted by

$$R_{\rm e} = R_0 \left(\frac{L_{\rm UV}}{L_0} \right)^{\beta}, \quad (10)$$

where R_0 is the effective radius at L_0, and β is the slope. We set $L_0 = L^*_{z=3}$, which corresponds to $M_0 = -21$ (Steidel et al. 1999). This equation can be rewritten as

$$\log_{10} R_{\rm e} = -0.4 \times \beta (M_{\rm UV} + 21) + \log_{10}(R_0). \quad (11)$$

We linearly fit the $\log_{10}(R_{\rm e})$–$M_{\rm UV}$ relation for galaxies brighter than $M_{\rm UV} = -14.5$ at each redshift. The best-fitting values for R_0 and β at $z \sim 5$–10 are shown in Table 2.

We see that the slope of the size–luminosity relation, β, does not significantly change at $z \sim 5$–9 and has a median value of $\beta \sim 0.25$ for galaxies with UV luminosity brighter than $M_{\rm UV} \sim -14$. This value agrees with observational studies for both local and high-redshift galaxies. For example, de Jong & Lacey (2000) found $\beta = 0.253 \pm 0.020$ for local spiral galaxies. Shen et al. (2003) derived a slope of $\beta \approx 0.26$ for the late-type galaxies from SDSS. Courteau et al. (2007) obtained $\beta = 0.321 \pm 0.010$ from local field and cluster spiral galaxies. Grazian et al. (2012) found $\beta = 0.3$–0.5 for LBGs at $z \sim 7$, while Holwerda et al. (2015) derived $\beta = 0.24 \pm 0.06$ using the Grazian et al. (2012) data. In addition, Huang et al. (2013) found $\beta = 0.22$ and 0.25 for the galaxies in GOODS and HUDF fields at $z \sim 4$ and $z \sim 5$, respectively. Finally, Shibuya et al. (2015) investigated the galaxy effective radius from a large *HST* sample and obtained $\beta = 0.27 \pm 0.01$ at $z \sim 0$–8. They also showed that β does not significantly evolve over this redshift range.

Due to limitations in sample volumes and selection biases, observed values of β often have large uncertainties and vary between studies. For example, observations are generally biased towards galaxies with high surface brightness and are not sensitive to

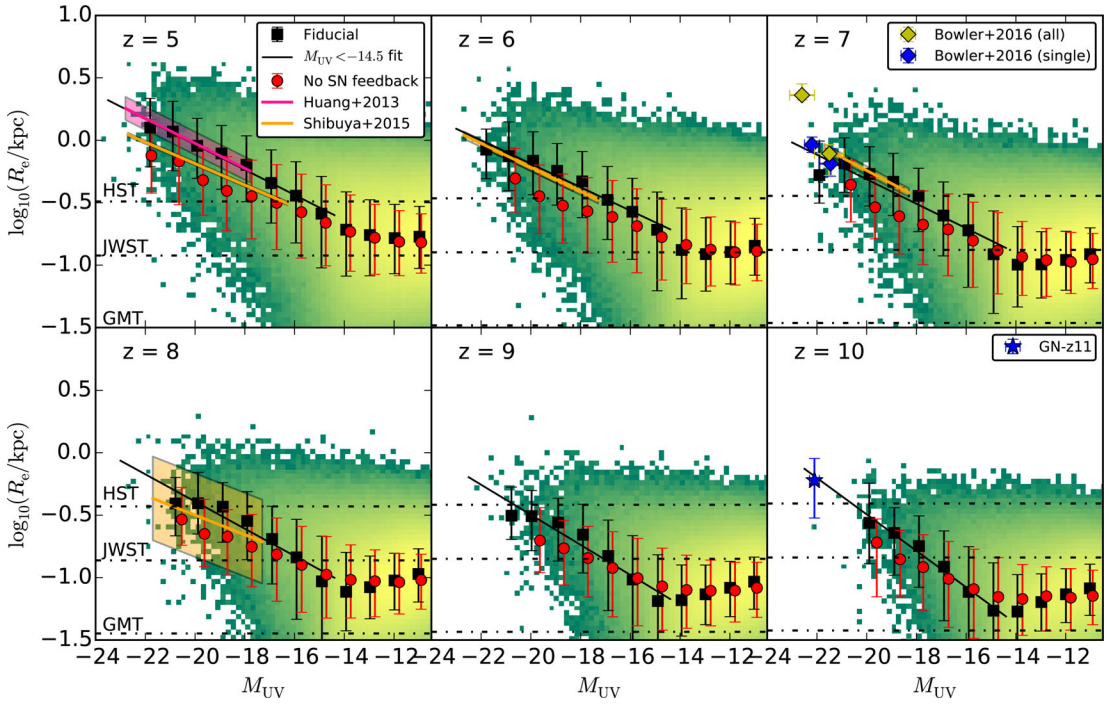

Figure 1. Effective radius of galaxies as a function of UV luminosity at $z \sim 5$–10. The colour profile shows the logarithm density of the distribution. The black squares and error bars represent the median and 16th to 84th percentiles of the R_e distribution in bins which contain at least 10 galaxies. The black solid lines are the linear best fits for galaxies with $M_{1600} < -14.5$, and are extended to brighter luminosities. The pink and orange lines and associated shaded regions show the observed relations from Huang et al. (2013) and Shibuya et al. (2015). The blue and yellow diamonds show the observations at $z \sim 7$ from Bowler et al. (2016). The blue star shows luminous galaxy GN-z11 found by Oesch et al. (2016). For model comparison, the red circles and error bars show the median and distribution of size–luminosity from the model with supernova feedback turned off. The dash–dotted lines represent the minimum measurable effective radii of *HST*, *JWST* and GMT.

Table 2. The best-fitting parameters R_0 and β (equation 10) for the model galaxies with UV magnitudes $M_{UV} < -14$ at $z \sim 5$–10.

z	R_0/kpc	β
5	1.17 ± 0.05	0.25 ± 0.02
6	0.80 ± 0.05	0.23 ± 0.02
7	0.61 ± 0.07	0.25 ± 0.04
8	0.53 ± 0.07	0.28 ± 0.04
9	0.42 ± 0.06	0.30 ± 0.04
10	0.45 ± 0.04	0.36 ± 0.03

measured properties of fainter, more spatially extended galaxies. Because a model does not suffer from these selection effects and can have a large sample of both bright and faint galaxies, we are able to investigate the true scatter of the size–luminosity relation.

The size–luminosity relation fitted to the model predictions is also consistent with the analytic prediction (equation 3) of Wyithe & Loeb (2011). In that work they considered a supernova feedback model where supernova-driven winds conserve momentum in the interaction with the galactic gas. The model results in a luminosity scaling of $a = 1/3$, which corresponds to $R_e \propto L^{0.25}$. While the model without supernova feedback yields $a = 0$, which corresponds to $R_e \propto L^{0.33}$.

To study the role of supernova feedback on the buildup of galaxy sizes, we show the size–luminosity relation for the no-supernova feedback model in Fig. 1 (red circles). The size–luminosity relation for the no-supernova feedback model is also flat at $M_{UV} > -14$. This is because the minimum size is set by the mass scale of efficient cooling in both models. There is no clear difference between the fiducial and no-supernova feedback model at $M_{UV} > -17$, where the accumulated effect from supernova feedback on star formation histories is not significant enough to be observed. However, at $M_{UV} < -17$, the median size of galaxies from the no-supernova feedback model is notably smaller than the fiducial model. In other words, for the same size galaxy, the no-supernova feedback model results in a much brighter luminosity. We note that removing supernova feedback allows more stars to form, and so the model has been recalibrated to produce the correct stellar mass density at $z = 5$. The luminosity difference is ~2–3 mag at $z = 5$–7, which is larger than the ~1 mag difference at $z = 8$–10. This is also due to the correct galaxy mass only being achieved at $z = 5$ in this recalibrated model.

The different size–luminosity relations from these two models arise because the supernova feedback in the fiducial model suppresses star formation resulting in a more gradual star formation history. In contrast, galaxies without supernova feedback have much burstier star formation histories and contain more young stellar populations which are UV bright. These effects are more significant at lower redshift due to the longer star formation histories. We also ran a simulation with both supernova and reionization feedback mechanisms switched off. However, we found the result to be almost identical to the no-supernova feedback model, with only a tiny difference at lower redshifts ($z \sim 5$–6).

4 RESOLVING GALAXIES WITH *HST*, *JWST* AND GMT

The spatial resolution of a telescope with effective diameter D_{tel} is

$$\Delta l = \Delta\theta d_A = \frac{1.22\lambda}{D_{tel}} d_A, \quad (12)$$

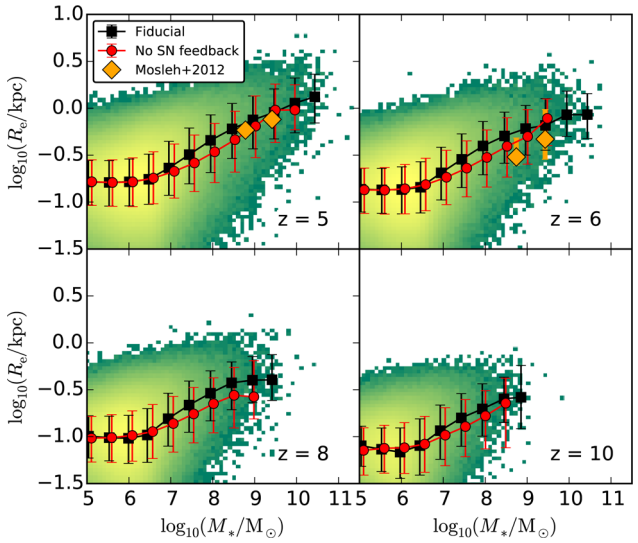

Figure 2. Size–mass relation of model galaxies at $z = 5, 6, 8, 10$. The colour profile shows the logarithm density of the distribution. The black squares and red circles show the median relation in bins which contain at least 10 galaxies. The error bars represent the median and 16th to 84th percentiles of the intrinsic scatter. The orange diamonds show the observations from Mosleh et al. (2012).

where $\Delta\theta$ is the angular resolution determined by the Rayleigh criterion, $\lambda = 1600(1 + z)$ Å is the observed wavelength of UV photons and d_A is the angular diameter distance. In equation (12), the observed wavelength is scaled by a factor of $(1 + z)$ at fixed intrinsic wavelength, the angular diameter distance decreases at a similar rate at $z \gtrsim 1$. Thus, the spatial resolution does not rapidly change with redshift. Galaxy sizes are usually measured through light profile fitting (e.g. Peng et al. 2002). As a result, one can trace the galaxy outskirt light, and obtain an effective radius below the spatial resolution of the telescope. The minimum observable size of a disc depends on many galaxy properties such as the light profile and the image depth. The comparison between the observed R_e and the spatial resolution limits of the *HST* indicates that values of R_e can be measured which are smaller than the resolution limit of the telescope by roughly a factor of ∼2 (e.g. Ono et al. 2013; Shibuya et al. 2015).

In Fig. 1, we show the minimum observable disc size R_{min} of *HST*, *JWST* and the GMT, where we adopt the relation $R_{min} \approx \Delta l/2$ as discussed above. We see that *HST* ($D_{tel} = 2.4$ m) can resolve the R_{min} of observed galaxies at $z \sim 5$–7, and the structures of typical $z > 8$ galaxies cannot be resolved. The larger diameter *JWST* ($D_{tel} = 6.5$ m) will resolve the R_{min} for galaxies brighter than $M_{UV} = (-14, -16, -18)$ at $z = (6, 8, 10)$. However, with an exposure time $t_{exp} = 10^6$ s, *JWST* will observe galaxies to $M_{UV} = (-15.0, -15.8, -16.3)$ with signal-to-noise ratio S/N = 10 at these redshifts, hence a significant fraction of $z > 8$ galaxies will be still unresolved. Due to the large mirror size, GMT ($D_{tel} = 25$ m) will have the ability to resolve all galaxies in haloes above the atomic cooling limit.

5 MASS–SIZE RELATION

Fig. 2 shows the relation between the effective radius and stellar mass of galaxies at $z \sim 5$, 6, 8 and 10 for both fiducial and no-supernova feedback models. Observed data from Mosleh et al. (2012) are also shown. The model size–mass relation is in good agreement with these observations. We see that for galaxies with stellar masses above $10^{6.5}$ M$_\odot$, more massive galaxies tend to have larger sizes. The galaxies from the fiducial model have larger sizes than the galaxies from no-supernova feedback model at fixed stellar mass. However, the difference in the size–mass relation between the fiducial and no-supernova feedback model is much smaller than in the size–luminosity relation. This is expected because we have tuned both models to produce the galaxy stellar mass density. However, star formation histories including supernovae lead to less variable UV luminosities resulting in larger difference seen in Fig. 1. For galaxies with $M_* < 10^{6.5}$ M$_\odot$, our two models show similar galaxy sizes due to the inefficient star formation in the minimum cooling mass, as was the case in the size–luminosity relation in Fig. 1.

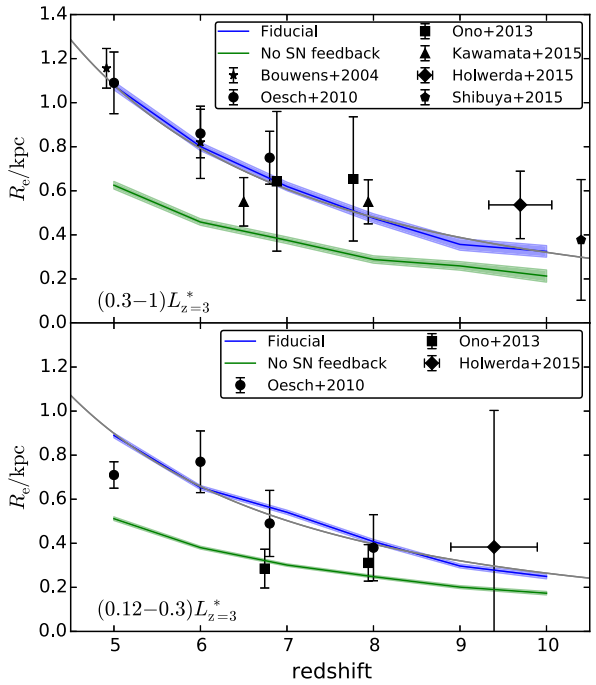

Figure 3. The redshift evolution of the mean effective radius for galaxies in the luminosity range $(0.3-1)L^*_{z=3}$ (upper panel) and $(0.12-0.3)L^*_{z=3}$ (lower panel). The blue line shows the mean effective radius from the fiducial model and the green line shows the mean effective radius from the model without supernova feedback. The shaded regions show the associated 1σ uncertainties of the means. The grey solid lines show the power-law fit to our model. For comparison, we show the observed mean sizes from Bouwens et al. (2004), Oesch et al. (2010), Ono et al. (2013), Kawamata et al. (2015), Holwerda et al. (2015) and Shibuya et al. (2015). We see that our fiducial model agrees with observations, while the no-supernova model significantly underestimates the galaxy sizes.

6 REDSHIFT EVOLUTION OF SIZES

The redshift evolution of galaxy sizes provides another important measurement in addition to the luminosity dependence (e.g. Bouwens et al. 2004; Ferguson et al. 2004; Oesch et al. 2010; Grazian et al. 2012; Ono et al. 2013; Holwerda et al. 2015; Kawamata et al. 2015; Shibuya et al. 2015). Fig. 3 shows the redshift evolution of the effective radius predicted by our model. To compare with observations of size evolution, galaxies were selected using their luminosity in ranges of $(0.3-1)L^*_{z=3}$ and $(0.12-0.3)L^*_{z=3}$. These luminosity ranges correspond to UV magnitudes from −21.0 to −19.7 and from −19.7 to −18.7, respectively. Both fiducial and

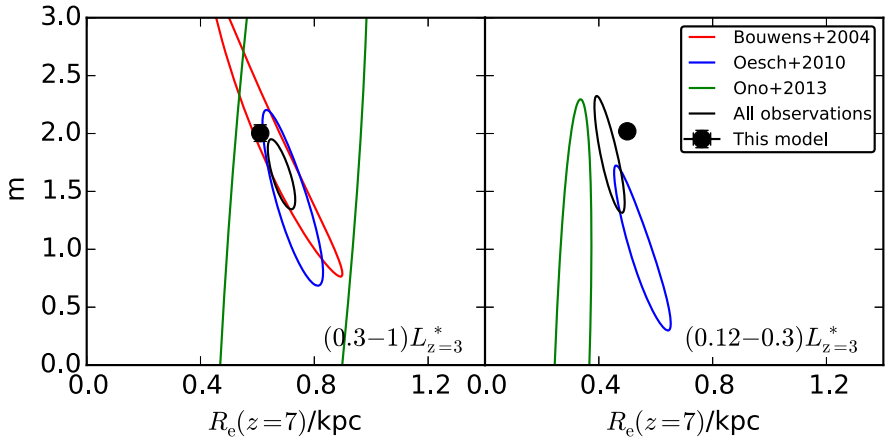

Figure 4. Confidence ellipses with $\Delta\chi^2 = 1$, which projects 1σ uncertainties on m and R_e axes. The red, blue and green contours are $z \gtrsim 5$ only observations from Bouwens et al. (2004), Oesch et al. (2010) and Ono et al. (2013), respectively. The black contours are from all observations shown in Fig. 3. Our best-fitting values are shown as black filled circles.

no-supernova feedback models are shown in the figure. For comparison, the observed galaxy sizes from Bouwens et al. (2004), Oesch et al. (2010), Ono et al. (2013), Kawamata et al. (2015), Holwerda et al. (2015) and Shibuya et al. (2015) are also shown.

We see that the evolution of galaxy sizes from our fiducial model is in good agreement with observations. However, the galaxy sizes in the no-supernova feedback model are underestimated at each redshift. For example, sizes at fixed luminosity in the no-supernova feedback model are ∼60 (70) per cent of those in the fiducial model at $z \sim 5$ (10). This corresponds to surface brightness densities which are ∼3 (2) times larger than the fiducial model prediction. These are distinguishable differences. To investigate the influence of parameter calibration in the no-supernova model, we have also run an uncalibrated no-supernova feedback simulation and found a qualitatively similar result. Therefore, we conclude that the galaxy-size evolution provides an additional observable for determining the importance of supernova feedback in early galaxy formation.

We fit the model size evolution at $z \sim 5$–10 using $R_e \propto (1+z)^{-m}$ and find $m = 2.00 \pm 0.07$ with $R_e(z=7) = 0.61 \pm 0.01$ kpc for galaxies with luminosity in the range $(0.3-1)L^*_{z=3}$ and $m = 2.02 \pm 0.04$ with $R_e(z=7) = 0.50 \pm 0.01$ kpc for galaxies with luminosity in the range $(0.12-0.3)L^*_{z=3}$. The fitted relations are shown as grey solid lines in Fig. 3. We also show $\Delta\chi^2 = 1$ confidence intervals using the observations from Bouwens et al. (2004), Oesch et al. (2010) and Ono et al. (2013), as well as combined observations from all data shown in Fig. 4. Here we only include the observational data at $z > 5$ and do not include more precise measurements at $z < 5$ which could dominate the fit.

We see that the fitted m from our model is comparable to observations. For example, $m = 1.64 \pm 0.30$ and 1.82 ± 0.51 are derived using the combined observations shown in Fig. 4 with luminosities in the ranges $(0.3-1)L^*_{z=3}$ and $(0.12-0.3)L^*_{z=3}$, respectively. We note that the fits from our model as well as $z > 5$ observations give larger values for m compared to observations that include $z < 5$ data as shown in Table 1. This may suggest that galaxy sizes undergo faster evolution at $z > 5$ compared to the evolution at lower redshift.

The normalization $R_e(z=7)$ for model galaxies with luminosity in the range $(0.12-0.3)L^*_{z=3}$ is slightly larger than the combined observations. However, these $z > 5$ observations are also inconsistent with each other due to the large uncertainties from the small sample. We find that $R_e(z=7)$ is in agreement with combined observations with 3σ uncertainty.

7 MEASURE OF GALAXY SIZE

Before concluding, we discuss the applicability of R_d as a measure of galaxy size. In observations, morphologies of LBGs are often found to be irregular and clumpy, sometimes showing multiple components (e.g. Giavalisco, Steidel & Macchetto 1996; Ravindranath et al. 2006; Guo et al. 2015; Bowler et al. 2016; Curtis-Lake et al. 2016; Shibuya et al. 2016). This could be due to two different formation mechanisms: (i) galaxy interactions, such as mergers (e.g. Lotz et al. 2006; Overzier et al. 2008); (ii) distributed and clumpy star formation regions within the same collapsing cloud due to instabilities (e.g. Goldader et al. 2002; Law et al. 2007; Dekel, Sari & Ceverino 2009; Oesch et al. 2010; Jiang et al. 2013; Behrendt, Burkert & Schartmann 2016).

Morphological studies at very high redshift are more challenging. Shibuya et al. (2016) investigated the evolution of clumpy galaxies with large *HST* samples and found that the clumpy fraction increases from $z \sim 0$ to 1 but subsequently decreases from $z \sim 1$–3 to 8. On the other hand, high-resolution cosmological simulations show that galaxies at $z \gtrsim 6$ are dominated by disc morphologies (e.g. Pawlik, Milosavljević & Bromm 2011; Romano-Díaz et al. 2011; Feng et al. 2015). For example, using the large-volume BLUETIDE simulation, Feng et al. (2015) found that at $z = 8$–10, up to 70 per cent of the galaxy population more massive than 10^{10} $M_\odot$ are disc galaxies. Detailed measurement of more compact and clumpy galaxies are limited by the angular resolution of instruments, and the origin of observed clumpy morphologies at high redshift is still under debate.

Bowler et al. (2016) recently published size measurements for a sample of extremely luminous galaxies at $z \sim 7$. Bowler et al. (2016) divided the sample into two groups (single and multicomponent) according to their morphologies. The size measurements are shown as the yellow (all galaxies) and blue (single component) diamonds in Fig. 1. We see that the size–luminosity relation for the single morphology galaxies is in good agreement with our model, while including clumpy morphology galaxies leads to larger sizes. This may suggest that the multicomponent galaxies are merging systems (Bowler et al. 2016). However, we are not able to rule out the clumpy-formation scenario due to the simplification of our

semi-analytic model. Also, limited by the volume and mass resolution of our *N*-body simulation, the bright multicomponent galaxies which undergo mergers will not be resolved by our model.

8 CONCLUSIONS

We have used the semi-analytic model MERAXES to study the dependence of galaxy size on UV luminosity, stellar mass and redshift at $z \sim 5$–10. We also studied the effect of supernova feedback on the evolution of galaxy sizes. We show that the rotationally supported disc model generally adopted in semi-analytic models can be used to study the sizes of high-redshift galaxies. Our primary findings are as follows.

(i) The effective radius scales with UV luminosity as $R_e \propto L^{0.25}$ for galaxies with luminosity $M_{UV} \lesssim -14$. Galaxies with the same disc size in the no-supernova feedback model have brighter UV magnitudes than in the fiducial model.

(ii) Our fiducial model with strong supernova feedback successfully reproduces the redshift evolution of average galaxy sizes at $z > 5$, which is slightly steeper than $z < 5$ observations. The model with no-supernova feedback produces a significantly smaller radius at fixed luminosity than the fiducial model.

(iii) The recently identified luminous galaxy GN-z11 at $z \sim 11$ (Oesch et al. 2016) lies on our model-fitted size–luminosity relation. The fitted relation is also in agreement with the size measurements of very luminous galaxies containing single components and with individual components of luminous multicomponent systems at $z \sim 7$ (Bowler et al. 2016).

(iv) A significant fraction of z > *8* galaxies will not be resolved by *JWST*. However, GMT will have the ability to resolve all galaxies in haloes above the atomic cooling limit.

We conclude that galaxy sizes provide an important additional constraint on galaxy-formation physics during reionization, and that current observations of galaxy size and evolution reinforce the importance of supernova feedback. These findings are in agreement with results based on the stellar mass function and luminosity function.

ACKNOWLEDGEMENTS

This research was supported by the Victorian Life Sciences Computation Initiative (VLSCI), grant ref. UOM0005, on its Peak Computing Facility hosted at the University of Melbourne, an initiative of the Victorian Government, Australia. Part of this work was performed on the gSTAR national facility at Swinburne University of Technology. gSTAR is funded by Swinburne and the Australian Governments Education Investment Fund. This research programme is funded by the Australian Research Council through the ARC Laureate Fellowship FL110100072 awarded to JSBW. AM acknowledges support from the European Research Council (ERC) under the European Union's Horizon 2020 research and innovation programme (grant agreement no. 638809 AIDA).

REFERENCES

Angel P. W., Poole G. B., Ludlow A. D., Duffy A. R., Geil P. M., Mutch S. J., Mesinger A., Wyithe J. S. B., 2016, MNRAS, 459, 2106
Behrendt M., Burkert A., Schartmann M., 2016, ApJ, 819, L2
Bouwens R. J., Illingworth G. D., Blakeslee J. P., Broadhurst T. J., Franx M., 2004, ApJ, 611, L1
Bouwens R. J. et al., 2014, ApJ, 793, 115
Bouwens R. J. et al., 2015, ApJ, 803, 34
Bower R. G., Benson A. J., Malbon R., Helly J. C., Frenk C. S., Baugh C. M., Cole S., Lacey C. G., 2006, MNRAS, 370, 645
Bowler R. A. A., Dunlop J. S., McLure R. J., McLeod D. J., 2016, preprint (arXiv:1605.05325)
Bryan G. L., Norman M. L., 1998, ApJ, 495, 80
Bullock J. S., Kolatt T. S., Sigad Y., Somerville R. S., Kravtsov A. V., Klypin A. A., Primack J. R., Dekel A., 2001, MNRAS, 321, 559
Carroll S. M., Press W. H., Turner E. L., 1992, ARA&A, 30, 499
Cole S., Lacey C. G., Baugh C. M., Frenk C. S., 2000, MNRAS, 319, 168
Courteau S., Dutton A. A., van den Bosch F. C., MacArthur L. A., Dekel A., McIntosh D. H., Dale D. A., 2007, ApJ, 671, 203
Cox T. J., Primack J., Jonsson P., Somerville R. S., 2004, ApJ, 607, L87
Croton D. J. et al., 2006, MNRAS, 365, 11
Curtis-Lake E. et al., 2016, MNRAS, 457, 440
de Jong R. S., Lacey C., 2000, ApJ, 545, 781
De Lucia G., Blaizot J., 2007, MNRAS, 375, 2
Dekel A., Sari R., Ceverino D., 2009, ApJ, 703, 785
Duncan K. et al., 2014, MNRAS, 444, 2960
Fall S. M., Efstathiou G., 1980, MNRAS, 193, 189
Feng Y., Di Matteo T., Croft R., Tenneti A., Bird S., Battaglia N., Wilkins S., 2015, ApJ, 808, L17
Ferguson H. C. et al., 2004, ApJ, 600, L107
Giavalisco M., Steidel C. C., Macchetto F. D., 1996, ApJ, 470, 189
Goldader J. D., Meurer G., Heckman T. M., Seibert M., Sanders D. B., Calzetti D., Steidel C. C., 2002, ApJ, 568, 651
González J. E., Lacey C. G., Baugh C. M., Frenk C. S., Benson A. J., 2009, MNRAS, 397, 1254
González V., Labbé I., Bouwens R. J., Illingworth G., Franx M., Kriek M., 2011, ApJ, 735, L34
Grazian A. et al., 2012, A&A, 547, A51
Grazian A. et al., 2015, A&A, 575, A96
Guo Y. et al., 2015, ApJ, 800, 39
Guo Q. et al., 2016, MNRAS, 461, 3457
Holwerda B. W., Bouwens R., Oesch P., Smit R., Illingworth G., Labbe I., 2015, ApJ, 808, 6
Huang K.-H., Ferguson H. C., Ravindranath S., Su J., 2013, ApJ, 765, 68
Jiang L. et al., 2013, ApJ, 773, 153
Kauffmann G., 1996, MNRAS, 281, 475
Kauffmann G., White S. D. M., Guiderdoni B., 1993, MNRAS, 264, 201
Kawamata R., Ishigaki M., Shimasaku K., Oguri M., Ouchi M., 2015, ApJ, 804, 103
Kennicutt R. C., Jr,1998, ApJ, 498, 541
Lacey C. G., Baugh C. M., Frenk C. S., Benson A. J., 2011, MNRAS, 412, 1828
Lacey C. G. et al., 2016, MNRAS, 462, 3854
Law D. R., Steidel C. C., Erb D. K., Pettini M., Reddy N. A., Shapley A. E., Adelberger K. L., Simenc D. J., 2007, ApJ, 656, 1
Leitherer C. et al., 1999, ApJS, 123, 3
Leitherer C., Ortiz Otálvaro P. A., Bresolin F., Kudritzki R.-P., Lo Faro B., Pauldrach A. W. A., Pettini M., Rix S. A., 2010, ApJS, 189, 309
Leitherer C., Ekström S., Meynet G., Schaerer D., Agienko K. B., Levesque E. M., 2014, ApJS, 212, 14
Liu C., Mutch S. J., Angel P. W., Duffy A. R., Geil P. M., Poole G. B., Mesinger A., Wyithe J. S. B., 2016, MNRAS, 462, 235 (Paper-IV)
Lotz J. M., Madau P., Giavalisco M., Primack J., Ferguson H. C., 2006, ApJ, 636, 592
Mesinger A., Furlanetto S., Cen R., 2011, MNRAS, 411, 955
Meurer G. R., Heckman T. M., Calzetti D., 1999, ApJ, 521, 64
Mihos J. C., Hernquist L., 1994, ApJ, 431, L9
Mihos J. C., Hernquist L., 1996, ApJ, 464, 641
Mo H. J., Mao S., White S. D. M., 1998, MNRAS, 295, 319
Mosleh M. et al., 2012, ApJ, 756, L12
Mutch S. J., Geil P. M., Poole G. B., Angel P. W., Duffy A. R., Mesinger A., Wyithe J. S. B., 2016a, MNRAS, 462, 250 (Paper-III)
Mutch S. J. et al., 2016b, MNRAS, 463, 3556
Navarro J. F., Frenk C. S., White S. D. M., 1997, ApJ, 490, 493
Oesch P. A. et al., 2010, ApJ, 709, L21

Oesch P. A. et al., 2016, ApJ, 819, 129
Oke J. B., Gunn J. E., 1983, ApJ, 266, 713
Ono Y. et al., 2013, ApJ, 777, 155
Overzier R. A. et al., 2008, ApJ, 677, 37
Pawlik A. H., Milosavljević M., Bromm V., 2011, ApJ, 731, 54
Peng C. Y., Ho L. C., Impey C. D., Rix H.-W., 2002, AJ, 124, 266
Planck Collaboration, 2015, A&A, 594, A13
Poole G. B., Angel P. W., Mutch S. J., Power C., Duffy A. R., Geil P. M., Mesinger A., Wyithe S. B., 2016, MNRAS, 459, 3025 (Paper-I)
Ravindranath S. et al., 2006, ApJ, 652, 963
Romano-Díaz E., Choi J.-H., Shlosman I., Trenti M., 2011, ApJ, 738, L19
Salpeter E. E., 1955, ApJ, 121, 161
Shankar F., Marulli F., Bernardi M., Boylan-Kolchin M., Dai X., Khochfar S., 2010, MNRAS, 405, 948
Shen S., Mo H. J., White S. D. M., Blanton M. R., Kauffmann G., Voges W., Brinkmann J., Csabai I., 2003, MNRAS, 343, 978
Shibuya T., Ouchi M., Harikane Y., 2015, ApJS, 219, 15
Shibuya T., Ouchi M., Kubo M., Harikane Y., 2016, ApJ, 821, 72
Smit R., Bouwens R. J., Franx M., Illingworth G. D., Labbé I., Oesch P. A., van Dokkum P. G., 2012, ApJ, 756, 14
Somerville R. S., Primack J. R., Faber S. M., 2001, MNRAS, 320, 504
Song M. et al., 2016, ApJ, 825, 5
Springel V., 2005, MNRAS, 364, 1105
Springel V., White S. D. M., Tormen G., Kauffmann G., 2001, MNRAS, 328, 726
Steidel C. C., Adelberger K. L., Giavalisco M., Dickinson M., Pettini M., 1999, ApJ, 519, 1
Stevens A. R. H., Croton D. J., Mutch S. J., 2016, MNRAS, 461, 859
Tonini C., Mutch S. J., Croton D. J., Wyithe J. S. B., 2016, MNRAS, 459, 4109
van den Bergh S., 2000, The Galaxies of the Local Group. Cambridge Univ. Press, Cambridge
Vázquez G. A., Leitherer C., 2005, ApJ, 621, 695
White S. D. M., Frenk C. S., 1991, ApJ, 379, 52
White S. D. M., Rees M. J., 1978, MNRAS, 183, 341
Wyithe J. S. B., Loeb A., 2011, MNRAS, 413, L38
Xie L., Guo Q., Cooper A. P., Frenk C. S., Li R., Gao L., 2015, MNRAS, 447, 636

This paper has been typeset from a TEX/LATEX file prepared by the author.